Nonlinear repolarization dynamics in optical fibers: transient polarization attraction

Victor V. Kozlov,[1,2,*] Julien Fatome,[3] Philippe Morin,[3] Stephane Pitois,[3] Guy Millot,[3] and Stefan Wabnitz[1]

[1]*Department of Information Engineering, Università di Brescia, Via Branze 38, 25123 Brescia, Italy*
[2]*Department of Physics, St.-Petersburg State University, Petrodvoretz, St.-Petersburg, 198504, Russia*
[3]*Laboratoire Interdisciplinaire Carnot de Bourgogne (ICB), UMR 5209 CNRS, Université de Bourgogne, 9 av. Alain Savary, 21078 Dijon, France*
**Corresponding author: victor.kozlov@email.com*

Received April 8, 2011; accepted May 24, 2011;
posted June 8, 2011 (Doc. ID 145592); published July 7, 2011

In this work, we present a theoretical and experimental study of the response of a lossless polarizer to a signal beam with a time-varying state of polarization (SOP). By lossless polarizer, we mean a nonlinear conservative medium (e.g., an optical fiber) that is counterpumped by an intense and fully polarized pump beam. Such a medium transforms input uniform or random distributions of the SOP of an intense signal beam into output distributions that are tightly localized around a well-defined SOP. We introduce and characterize an important parameter of a lossless polarizer—its response time. Whenever the fluctuations of the SOP of the input signal beam are slower than its response time, a lossless polarizer provides an efficient repolarization of the beam at its output. Otherwise, if input polarization fluctuations are faster than the response time, the polarizer is not able to repolarize light.

OCIS codes: 230.5440, 060.4370, 230.1150, 230.4320.

1. INTRODUCTION

Over the last few years there has been a great deal of interest in the development of polarization-selective devices for nonlinear optics and telecom applications. The simplest and most common way to select a desired polarization state out of a laser source or from a telecom link is to insert a linear polarizer. A "standard" linear polarizer outputs only one polarization state. So one particular state of linear polarization input will experience 100% transmission, and the input of all others will experience a reduced transmission equal to the square of the fraction of the input wave's electric field vector projection along the "pass" direction of the linear polarizer. Clearly a beam with constant intensity but a time-fluctuating state of polariztion (SOP) may acquire large intensity fluctuations after passing through a linear polarizer, possibly resulting in significant degradation of the signal-to-noise ratio after detection. In addition, polarization-dependent losses may be detrimental when using nonlinear optical devices. In this work, we study the nonlinear lossless polarizer (NLP), a device that transforms all (or most) polarizations of the input beam into approximately one and the SOP at its output, without introducing any polarization-dependent losses.

Three types of NLPs for controlling the light SOP have been proposed so far. Historically, the first lossless polarizer was proposed and experimentally demonstrated in [1], where the effect of two-wave mixing in a photorefractive material was used for the amplification of a given polarization component of a light beam by using the orthogonal component as a pump beam. However, the use of such a device in telecommunication applications is limited by the intrinsically slow (of the order of seconds and minutes) response time inherent to photorefractive crystals. In this respect, it appears that NLPs based on the Kerr nonlinearity of optical fibers are more promising for fast SOP control. Indeed, a fiber-based NLP was experimentally demonstrated in a practical configuration involving a 20 km long, low-polarization-mode dispersion telecom (randomly birefringent) fiber, counterpumped with a 600 mW continuous wave (CW) beam [2]. This NLP was able to smooth at its output microsecond-range polarization bursts of the input 300 mW signal beam. A recent theoretical study has analyzed the CW operation of an NLP in the presence of random fiber birefringence [3]. The third type of lossless polarizers are also based on a Kerr medium, but do not require a counterpropagating beam. Here the spontaneous polarization, which is induced by natural thermalization of incoherent light in the nonlinear medium, lies at the heart of the repolarization mechanism [4].

In this paper, we devote our attention to the second class of NLPs. Their principle of operation is based on the so-called polarization attraction effect: virtually any input SOP of the signal beam is attracted to the vicinity of a definite SOP toward the device output. When visualized on the Poincaré sphere, all SOPs that are initially randomly (or uniformly) distributed over the entire Poincaré sphere contract into a small well-localized spot. The size of this spot, which is measured in terms of the degree of polarization (DOP) D,

$$D = \frac{1}{S_0}\sqrt{\sum_{i=1}^{3}\langle S_i\rangle^2} \tag{1}$$

(the smaller the size, the higher the DOP), quantifies the performance of an NLP. In Eq. (1), the average of the Stokes parameters that describe the SOP of a beam is performed as either a time or an ensemble average, as discussed in detail in Section 3. A practically relevant question involves the choice of the nonlinear fiber. Historically, the first fiber-based NLP

was realized in isotropic fibers; see [5,6]. The disadvantage of this setup is in the necessity to use high-power (~50 W) beams in order to obtain an efficient nonlinear interaction of two counterpropagating beams over a highly nonlinear fiber span of only 1–2 m (for the corresponding theory, see [7–10]). A bold step forward toward the practical use of these devices was provided by the recent experimental demonstration of lossless polarization attraction in a 20 km long telecommunication fiber: such a configuration permits 2 orders of magnitude reduction in the pump (and signal) power [2]. This solution is versatile, cheap, and easily integrable with most optoelectronic devices. As theoretically demonstrated in [11], lossless polarizers can also be implemented with a relatively shorter (~100 m) sample of highly nonlinear high birefringent or unidirectionally spun fiber.

The theoretical model presented in [3] unites all types of fibers (isotropic, deterministically birefringent, randomly birefringent, and spun) under one umbrella by showing that the propagation of counterpropagating beams in silica fibers is described by the same evolution equations: different fibers lead to specific values of the coefficients entering these equations. Fiber-based NLPs have different performances, but all exhibit the effect of polarization attraction under similar conditions of operation. Driven by practical considerations, we choose to work here with a telecommunication (i.e., randomly birefringent) fiber. Although, so far, the most studied case involves isotropic fibers, the theory that has been developed for these fibers cannot be directly applied to telecommunication fibers for reasons to be discussed over the next sections.

The literature available so far on telecommunication fiber-based NLPs [2,3] was mainly aiming at the proof-of-principle experimental and theoretical demonstration of the polarization attraction effect. Here we set our goal in substantially extending these results by characterizing through both numerical simulations as well as experiments the temporal polarization dynamics of NLPs. In Section 2, we formulate the model for the interaction of time-varying, counterpropagating beams in a randomly birefringent optical fiber, and provide the definition of the response time of an NLP. In Section 3, we provide, first, the definition of the two types of input signals that will be considered in this work, namely, input unpolarized light or scrambled light. In Subsection 3.A, we analyze the temporal response of the NLP to an input polarized beam, and reveal the possibility of obtaining periodic or even irregular temporal oscillations of the output SOP in correspondence of a CW input beam. Next, in Subsection 3.B, we present extensive numerical simulations where we compare ensemble and temporal averaging of the output SOP in the presence of either scrambled or unpolarized signals, respectively. We show that, whenever the time variations of the input unpolarized light are slow with the respect to the NLP response time, the repolarization by the NLP is ergodic in the sense that ensemble and time averages lead to virtually identical results. However, this property no longer holds when the time variation of the input unpolarized light is faster than the response time: in this situation, the repolarization property of the NLP no longer holds. In order to further investigate this point, we have numerically and experimentally investigated in Sections 3.A and 4 the repolarization action of an NLP upon a short input polarization fluctuation (or burst), as a function of the relative duration of the burst with respect to the response time. Simulations and experiments demonstrate with excellent agreement that uniform repolarization by the NLP requires polarization burst durations longer than the NLP response time. A discussion and conclusion is finally presented in Section 5.

2. MODEL EQUATIONS

The formulation of a model for describing the interaction of two counterpropagating and arbitrarily polarized beams in a Kerr medium with randomly varying birefringence in terms of deterministic coupled differential equations is not a trivial task. Indeed, such a formulation requires the accurate evaluation of statistical averages, and it involves a number of assumptions. In our approach, we make two main assumptions. The first hypothesis is that, among the two characteristics of the birefringence when represented as a three-dimensional vector, namely, its magnitude and its orientation, the magnitude is fixed at a constant value along the total fiber length L. On the other hand, we suppose that the orientation varies randomly with distance, with a characteristic correlation length L_c. The second assumption is that the fiber length $L \gg L_c$.

Based upon these two assumptions, one obtains a system of differential equations with variable coefficients for describing the mutual polarization coupling of two counterpropagating waves [3]. We may argue that, in order to obtain a significant repolarization effect, the differential beat length $L_B' \equiv [L_B^{-1}(\omega_s) - L_B^{-1}(\omega_p)]^{-1}$ should obey the inequality $L_B' \gg L$, where $L_B(\omega_s)$ $[L_B(\omega_p)]$ is the beat length at the signal (pump) frequency $\omega_s(\omega_p)$. In fact, if the previous inequality is not satisfied, then the polarizations of the two beams are scrambled by linear birefringence before significant nonlinear attraction may take place. In the limit $L/L_B' \to 0$, the polarization coupling coefficients are no longer variable, and we are left with a set of equations with constant coefficients. These equations are conveniently formulated in Stokes space as

$$\partial_\xi \mathbf{S}^+ = \mathbf{S}^+ \times J_s \mathbf{S}^+ + \mathbf{S}^+ \times J_x \mathbf{S}^-, \tag{2}$$

$$\partial_\eta \mathbf{S}^- = \mathbf{S}^- \times J_s \mathbf{S}^- + \mathbf{S}^- \times J_x \mathbf{S}^+. \tag{3}$$

For details of the derivation, see [3]. Here $\xi = (vt + z)/2$ and $\eta = (vt - z)/2$ are propagation coordinates, where v is the phase speed of light in the fiber. The sign "×" denotes vector product. The above equations are written for the three components, $S_1^\pm = \phi_1^{\pm *}\phi_2^\pm + \phi_1^\pm \phi_2^{\pm *}$, $S_2^\pm = i(\phi_1^{\pm *}\phi_2^\pm - \phi_1^\pm \phi_2^{\pm *})$, and $S_3^\pm = |\phi_1^\pm|^2 - |\phi_2^\pm|^2$, of the signal $\mathbf{S}^+ = (S_1^+, S_2^+, S_3^+)$ and the pump $\mathbf{S}^- = (S_1^-, S_2^-, S_3^-)$ Stokes vectors, respectively. Here $\phi_{1,2}^\pm$ are the polarization components of the signal and pump fields in the chosen reference frame. Self- and cross-polarization modulation (SPM and XPM) tensors are both diagonal and have the forms $J_s = \gamma_{ss}\mathrm{diag}(0,0,0)$ and $J_x = \frac{8}{9}\gamma_{ps}\mathrm{diag}(-1,1,-1)$. Note that the condition $L_B' \gg L$ implies that the carrier wavelengths of the pump and signal beams are close to each other (i.e., their wavelength spacing does not exceed ~1 nm). Therefore, $\gamma_{ss} \approx \gamma_{ps} \approx \gamma$, where γ denotes the nonlinear coefficient. In our model, the second- and higher-order group velocity dispersions are not taken into account for the reason that the pump and signal beams are considered quasi-CW. In other words, temporal modulations of the signal

SOP beam are supposed to be relatively slow, so that dispersive effects can be neglected over the distances involved in our study.

For each beam, we define the zeroth Stokes parameters S_0^+ and S_0^- according to the equation

$$S_0^{\pm} = \sqrt{(S_1^{\pm})^2 + (S_2^{\pm})^2 + (S_3^{\pm})^2}. \tag{4}$$

These parameters represent the power of the forward and backward beams, respectively. Since we are dealing with wave propagation in a lossless medium, the sum of the powers of both beams is a conserved quantity along the fiber length. Moreover, the equations of motion in Eqs. (2) and (3) imply that the powers of each beam are separately conserved: $S_0^+(z-ct) = S_0^+(z=0,t)$ and $S_0^-(z+ct) = S_0^-(z=L,t)$ for all z.

Henceforth, we shall be dealing only with uniform (i.e., independent of z) initial conditions. These are related to the boundary conditions at $t=0$ as follows:

$$S_i^+(z=0,t) = S_i^+(z,t=0), \tag{5}$$

$$S_i^-(z=L,t) = S_i^-(z,t=0), \tag{6}$$

with $i=1,2,3$. The choice of the initial conditions influences only the short-term polarization evolutions of the two beams, as they have no influence on the long-term behavior of the polarization states. It is precisely such long-term evolution that is of interest to us. Therefore, from now on, we shall specify only the boundary conditions: for the initial conditions, we may refer to the previous relationships as given in Eqs. (5) and (6).

Let us also introduce the nonlinear length $L_{NL} = (\gamma S_0^+)^{-1}$, which has the meaning of the characteristic length of nonlinear beam evolution inside the fiber. In its turn, the characteristic time is simply defined as $T_{NL} = L_{NL}/v$. In our simulations, we use L_{NL} as the unit for measuring distances in the fiber medium in a reference frame with the origin ($z=0$) at the left boundary, where we set the boundary conditions for the forward (signal) beam. At the right boundary (i.e., at $z=L$), we set the boundary conditions for the backward (pump) beam. The temporal scale in units of T_{NL} is used for measuring time. In simulations to be carried out in the Section 3, we set the total fiber length equal to $L=5L_{NL}$. We varied the pump power in the range $[1,5.5]S_0^+$. Whenever the pump power drops below S_0^+, the effect of polarization attraction quickly degrades; therefore, the power range $[0,1]S_0^+$ is not of interest here.

3. NUMERICAL SIMULATIONS

In the numerical study of polarization attraction, two different approaches can be distinguished. The first approach is the study of the response of the polarizer to input scrambled beams. By scrambled beams, we understand a set of N beams, where each individual beam is fully polarized, but the ensemble of the N SOPs is randomly or uniformly distributed over the entire Poincaré sphere. So, the DOP of the ensemble of beams is exactly zero. In this case, we compute the SOP of the outcoming signal beam, after its interaction with the nonlinear fiber pumped by the backward-propagating beam. We performed the integration of Eqs. (2) and (3) based on the numerical method that was proposed in [12]. The outcoming set of SOPs are averaged, as explained in Appendix A, so that the mean SOP and the DOP can be obtained. The repolarization property of the polarizer then leads to an output DOP that is different from zero. Note that the repolarization quality of the NLP depends on the specific polarization of the pump beam. In [3], we considered a set of pump beam SOPs that are represented on the Poincaré sphere by points in the vicinity of its six poles, namely, $(\pm1,0,0)$, $(0,\pm1,0)$ and $(0,0,\pm1)$. We observed that, in the last two cases, the NLP works relatively better than in the first four cases. However, the basic features of the polarization attraction do not critically depend on the choice of the pump SOP (even though significant variations in the output signal DOP may result when the pump SOP is varied). Therefore, in the following simulations, we will restrict our attention for simplicity to the case of a pump SOP equal to $(0.99,0.1,0.1)$. In this case, the signal SOP is, on average, attracted to a point in the vicinity of the pole $(-1,0,0)$.

This approach permits us to calculate the average response of the polarizer to any signal SOP in the stationary regime. That is, we obtain the output SOP long after all transient processes have died away. The studies of NLPs that were undertaken in [3,11] are based on this approach, which we term Approach S (scrambled).

An alternative approach involves the study of the response of an NLP to unpolarized light. By unpolarized light, we mean a beam whose the SOP is randomly varying in time on the scale of some characteristic correlation time T_c. Whenever the observation time T largely exceeds T_c, so that the coverage of the Poincaré sphere by the beam's SOP is uniformly achieved, then the (time-averaged) DOP is also zero. In this paper, we develop this approach and call it Approach U (unpolarized).

In Approach S we perform the ensemble average, while in Approach U we perform a time average. If these two statistical approaches yield identical results, then we may say that the system is ergodic. The numerical verification of the ergodicity of an NLP is the goal of the next subsection.

A. Response to Polarized Light

An ultimate goal of our simulations is to characterize the response of an NLP to a signal beam whose SOP is modulated in time with a characteristic frequency ω_m, thus mimicking the statistics of an unpolarized beam. The three Stokes parameters of the input signal beam are specified by the two angles α_1 and α_2 (which define the position of the tip of the Stokes vector on the Poincaré sphere) as follows:

$$S_1^+(z=0,t) = S_0^+ \sin\alpha_1(t)\cos\alpha_2(t), \tag{7}$$

$$S_2^+(z=0,t) = S_0^+ \sin\alpha_1(t)\sin\alpha_2(t), \tag{8}$$

$$S_3^+(z=0,t) = S_0^+ \cos\alpha_1(t). \tag{9}$$

We choose to vary these angles in time according to the linear law:

$$\alpha_1 = \alpha_0 + 2.53\omega_m t, \tag{10}$$

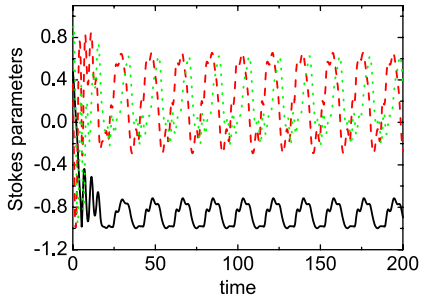

Fig. 1. (Color online) Stokes parameters of the signal beam at $z = L$ as a function of time: S_1^+ (black solid curve), S_2^+ (red dashed curve), and S_3^+ (green dotted curve). Time is measured in units T_{NL}. Stokes parameters are normalized to S_0^+; $S_0^- = 3S_0^+$.

$$\alpha_2 = \alpha_0 - 3.53\omega_m t. \tag{11}$$

For observation times $T \gg \omega_m^{-1}$, it can be easily verified that the tip of the input Stokes vector almost uniformly covers the entire Poincaré sphere. Indeed, for $T = 50\omega_m^{-1}$, the time-averaged input beam DOP is as low as 0.0074, which is low enough to consider the beam as virtually unpolarized.

Before coming to the consideration of input unpolarized beams, we find it instructive to treat the response of the NLP to fully polarized light: we may set, for example, $\omega_m = 0$ and $\alpha_0 = \pi/4$. First of all, let us observe the signal SOP at the fiber output end (at $z = L$) as a function of time. After a short transient process, we observed that the Stokes vector components enter a regime of fully periodic oscillations, as demonstrated in Fig. 1. Depending on the input SOP, these temporal oscillations may have larger or smaller amplitude. For some input SOPs, we observed a time stationary output. No other (for instance, chaotic, as earlier reported in the case of isotropic fibers; see [13]) regimes were detected at least for the limited range of pump and signal powers considered here. Also note that, as expected and in spite of the oscillations, the tip of the output signal SOP is, on average, attracted to a point that is located in the vicinity of the pole $(-1, 0, 0)$.

Figure 2 illustrates spatial distributions along the fiber length of the Stokes components of the signal at four successive times. Here we consider the same parameters that were used for generating Fig. 1. The four snapshots in Fig. 2 exactly cover one period of the temporal oscillations in Fig. 1. Indeed, the time step between the snapshots is $\Delta t = 6T_{NL}$: the first snapshot is taken at $t = 30T_{NL}$ and the last at $t = 48T_{NL}$. Figure 2 demonstrates how the Stokes components "breath" all across the fiber except for the input end, where the SOP is clamped by the imposed stationary boundary conditions.

The period of oscillations of the Stokes parameters decreases with larger pump power, as demonstrated in the left panel of Fig. 3. The periodic regime suddenly starts at $S_0^- = 1.9S_0^+$ (for our particular choice of signal and pump SOPs): below this pump power value the polarization evolution regime is purely stationary. We may argue that the system experiences a Hopf bifurcation; however, a detailed study of the bifurcation diagram by methods of nonlinear dynamics is beyond the scope of this paper.

The practical consequence of the periodic temporal oscillations of the Stokes parameters for pump powers larger than $1.9S_0^+$ is the depolarization of the signal at the fiber output end. In the specific case discussed here, an input fully polarized beam with DOP = 1 transforms into an output partially polarized beam with DOP = 0.9, as demonstrated in the right panel of Fig. 3. Here the DOP is calculated as

$$D_U(T) = \frac{1}{T}\frac{1}{S_0^+}\sqrt{\sum_{i=1}^{3}\left[\int_0^T \mathrm{d}t S_i^+(L,t)\right]^2}. \tag{12}$$

Here, the index U is associated to a time average (over a time interval T much larger than T_{NL}) that is characteristic of the previously defined Approach U. In situations where larger amplitude oscillations of the SOP of the output signal occur, the corresponding DOP is further reduced and may, in principle, even drop below 0.1, as we shall see in Subsection 3.B. From these observations, we deduce a rather unexpected behavior for a polarizer: namely, it transforms a fully polarized beam into a partially polarized or even, for some choice of parameters, an almost unpolarized beam. Such a property of fractional and deterministic depolarization of fully polarized beams may find some interesting applications in nonlinear photonic devices.

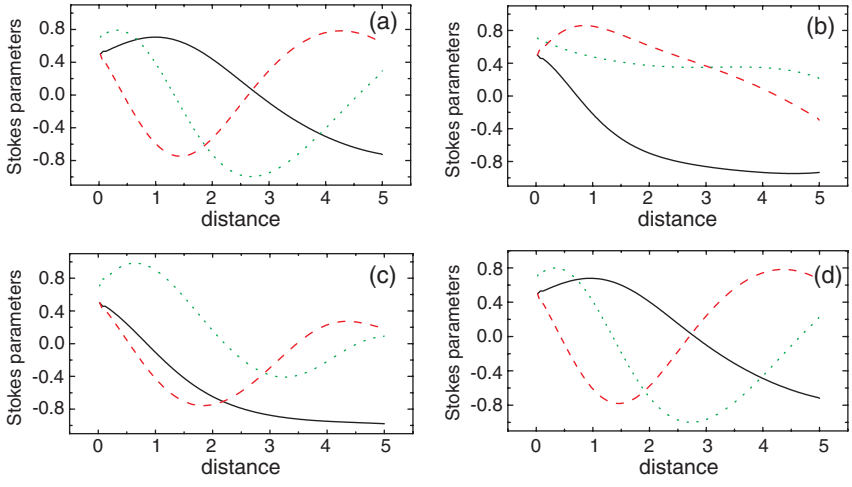

Fig. 2. (Color online) Stokes parameters of the signal beam inside the medium at four instants of time: (a) $t = 30$, (b) $t = 36$, (c) $t = 42$, and (d) $t = 48$. S_1^+ (black solid curve), S_2^+ (red dashed curve), and S_3^+ (green dotted curve). Time is measured in units T_{NL}. All Stokes parameters are normalized to S_0^+. Parameters are as in Fig. 1. The four snapshots cover exactly one period of the oscillations that are shown in Fig. 1.

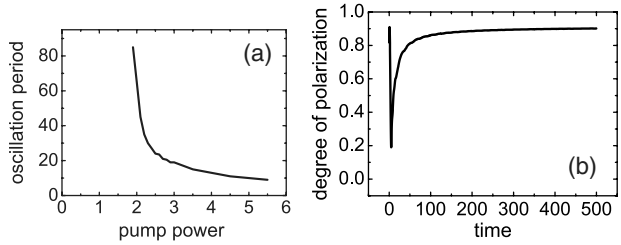

Fig. 3. (a) Period (in units of T_{NL}) of the Stokes parameter oscillations at $z = L$ versus pump power (in units of S_0^+). (b) DOP versus time for the same case as in Figs. 1 and 2.

Note that the previously described depolarization property of the NLP does not stand in contradiction with its main feature, i.e., the capability to repolarize light. As a matter of fact, the present NLP does not act as a perfect polarizer, in the sense that it only pulls input SOPs toward the vicinity of some point, but not exactly to a given point on the Poincaré sphere. As we shall see in Subsection 3.B, this particular NLP would transform initially unpolarized light into a partially polarized beam with DOP = 0.74. This value is the main statistical characteristic of the polarizer. On the other hand, whenever an NLP is fed not by unpolarized light but by fractionally polarized light or even fully polarized light, its performance remains to a large extent unpredictable. Indeed, the output DOP may turn out to be larger or substantially less than 0.74, in a manner that sensitively depends on the size and location of the spot of input SOPs on the Poincaré sphere.

In conclusion, we may note that the time scale for reaching a stationary DOP value, as observed in the right panel of Fig. 3, is of 1 order of magnitude larger than the time required for entering the regime of perfectly periodic oscillations of the Stokes parameters as shown in Fig. 1. The relatively long relaxation time (say, T_D) toward the stationary DOP is related to the fact that its value is virtually independent of the initial polarization states of the beams. From our simulations, we estimate that T_D is typically equal to $100T_{NL}$. In statistics, processes with time-invariant mean values are characterized as stationary. In all our numerical studies, we employed relatively long observation times to make sure that the long-term dynamics of the average values does not depend on time, as we are only dealing here with stationary processes.

B. Response to Unpolarized Light

Let us study now the response of a fiber NLP when fed with unpolarized light at its input. In order to numerically simulate an unpolarized signal, we replace the previously considered stationary boundary conditions at $z = 0$ with the time-varying polarization state as specified by Eqs. (7)–(11). Quite interestingly, as we shall see, the repolarization capabilities of the NLP sensitively depend upon the relative value of the input signal modulation frequency ω_m and what can be defined as the cutoff frequency of the NLP response, or $\omega_c = T_{NL}^{-1}$. Just as for the case that was illustrated in Fig. 1, a time interval of the order of a dozen units of T_{NL} is typically enough for reaching an equilibrium (either periodic in time, or stationary) state for the Stokes parameters of the signal and pump beams across the entire fiber. Therefore, whenever the input signal polarization modulation frequency is smaller than the NLP cutoff frequency (i.e., $\omega_m T_{NL} \ll 1$) one obtains that the response of the NLP is quasi-stationary. In this situation, at any instant of time, the pump and signal beams along the fiber are in equilibrium with each other. Such an equilibrium distribution of polarization states is what we call a polarization attractor. In our study, we are going to deal with both stationary and time-periodic polarization attractors.

In Approach S (dealing with averaging the response of the NLP over scrambled beams), the output SOP of each signal beam from the ensemble was detected long after all transient processes have died away and an equilibrium state (i.e., independent of initial conditions) was established for both the signal and the pump beams. Thus, in both Approach S with detection times $T \gg T_{NL}$ on the one hand, and Approach U considered in the limit of $\omega_m T_{NL} \ll 1$ and observation times $T > \max(50\omega_m, T_D)$ (these conditions are necessary for modeling the unpolarized beam at the input and at the same time obtaining the long-term value of its output DOP) on the other hand, we are going to deal with equilibrium states for beams inside the fiber. Also, in both approaches, we are going to scan the input SOPs across the entire Poincaré sphere. Thus, we may expect that the statistical averages computed with either Approach S or Approach U are going to be identical. By statistical averages, we mean the average values of the three Stokes parameters of the signal and its DOP. Figure 4 shows that the results of the two approaches are indeed relatively close to each other: the small discrepancies may be attributed to statistical fluctuations. The details of the statistical data processing for Approach S are presented in Appendix A.

The mean values of the Stokes vector components in Approach U are simply computed as the time averages:

$$\langle S_i^+(L,T)\rangle_T = \frac{1}{T}\int_0^T \mathrm{d}t S_i^+(L,t), \tag{13}$$

with $i = 1, 2, 3$. Next, the DOP is computed as given by Eq. (12): the value shown in Fig. 4 is exactly the long-term DOP = 0.74 (for $S_0^- = 3S_0^+$) for initially unpolarized beams, which was mentioned in Subsection 3.A.

Let us come back from the comparison of Approaches S and U to consider Approach U in more detail. For example, we may observe the temporal dynamics of the output S_1^+ Stokes component of the signal at $z = L$ whenever its input SOP changes adiabatically (i.e., $\omega_m T_{NL} \ll 1$). In Fig. 5, we can see that the output first Stokes component is predominantly localized in the lower part of the graph. Indeed, for

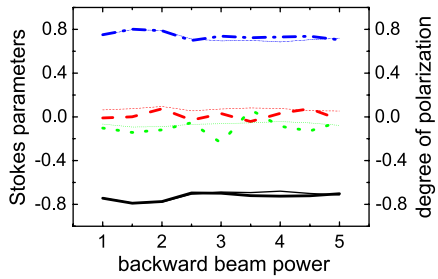

Fig. 4. (Color online) Components of the mean Stokes vector and the DOP of the output signal beam as a function of the relative power of the backward beam: S_1^+ (black solid curve), S_2^+ (red dashed curve), S_3^+ (green dotted curve), and DOP (blue dashed–dotted curve), for the input SOP of the pump beam: $(0.99, 0.1, 0.1)$. Thick (thin) curves are calculated with Approach S (U). The Stokes parameters are normalized with respect to $S_0^+(z,t)$. The observation time in Approach U is $T = 50\omega_m^{-1} = 250000T_{NL}$ and $\omega_m T_{NL} = 0.0002$. The observation time in Approach S is $T = 10000T_{NL}$ and $N = 110$.

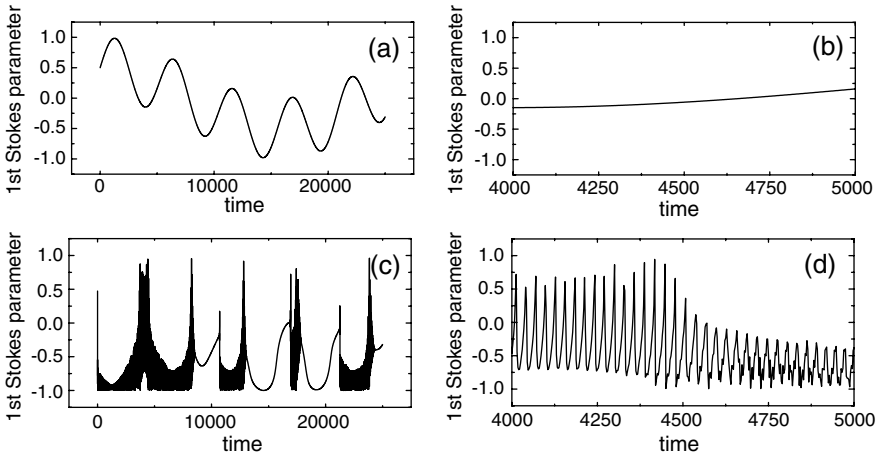

Fig. 5. The first component S_1^+ of the input and output Stokes vector of the signal beam as a function of time: (a), (b) input; (c), (d) output. (b) and (d) are the exploded views of (a) and (c). The first Stokes component is normalized with respect to $S_0^+(z,t)$. The observation time $T = 50\omega_m^{-1}$; $\omega_m T_{NL} = 0.0002$; $S_0^- = 3S_0^+$.

the pump SOP considered here, the average output signal SOP is attracted to the vicinity of the $(-1,0,0)$ pole on the Poincaré sphere; see [3]. However, Fig. 5 also shows that some input SOPs lead to strong spikes in the output SOP, indicating that these SOPs are not attracted by the polarizer. Such events are relatively rare. Overall, the output DOP is 0.74. Large excursions of the output SOP from the attraction point can be detrimental whenever they occur in polarization-sensitive telecom links. In order to avoid them, setups with larger values of DOP should be selected, where such spikes are much less likely. For instance, DOP can be as high as 0.99 for polarizers based on high birefringence or spun fibers [11]. Also, in [3], the DOP = 0.9 was found for polarizers based on the telecom fibers that we study here, whenever the pump beam SOP is in the vicinity of the pole $(0,0,1)$ or $(0,0,-1)$. In this paper, we are interested in studying the time-dependent dynamics or transient properties of lossless polarizers, and not in their optimization. Therefore, high and low output DOPs are equally good for the present purposes.

Figure 5 also demonstrates that, for the pump power value $S_0^- = 3S_0^+$, the output signal SOP predominantly exhibits oscillatory behavior, although intervals with a stationary response are also present.

So far we were interested in the adiabatic regime, when $\omega_m T_{NL} \ll 1$ and the counterpropagating beams are in equilibrium at any instant of time. An interesting question is: is the polarizer still effective with higher modulation frequencies, i.e. whenever $\omega_m T_{NL} \sim 1$? In this case, signal and pump beams do not have sufficient time to reach an equilibrium state across the fiber. As a consequence, as seen in Fig. 6, the DOP quickly degrades whenever $\omega_m T_{NL}$ approaches unity. Therefore, we may conclude that it is the presence of a steady-state equilibrium (polarization attractor) between the signal and pump beams that enables the NLP to work. In other words, a signal beam with an input SOP fluctuating faster than T_{NL} will not be effectively repolarized by the polarizer.

In addition to the previous statistical description, it is instructive to study how the polarizer responds to a fast burst of the input signal SOP that is imposed on the otherwise fully polarized signal beam. Such a burst can be modeled by imposing a brief disturbance on the angles α_1 and α_2:

$$\alpha_1 = \alpha_0 + \pi \mathrm{sech}[2.53(\omega_m t - 125)], \tag{14}$$

$$\alpha_2 = \alpha_0 - \frac{\pi}{2}\mathrm{sech}[3.53(\omega_m t - 125)], \tag{15}$$

with $\alpha_0 = \pi/4$ and $\omega_m = T_{NL}^{-1}$. Figure 7 shows that the burst is not compensated by the NLP and it survives the propagation, so that the output Stokes component S_1^+ is disturbed as severely as the input one. However, this disturbance is as brief as the input one. This observation means that the equilibrium state of the signal and the pump beams that is established across the fiber is only locally perturbed and it is immediately recovered after the burst has passed. This resistance to fast perturbations is a natural consequence of the fact that the NLP cannot react faster than its characteristic response time T_{NL}.

In practice, the NLP response time may be controlled by varying the input signal power. Therefore, at least in principle, an input polarization burst of arbitrary short temporal duration (say, T_b) may always be compensated by the NLP as long as the input signal power becomes sufficiently large (so that $T_b > T_{NL}$). Such a situation is presented in Fig. 8, where we display the output value of the S_1^+ parameter as a function of the signal power (measured by the number of nonlinear

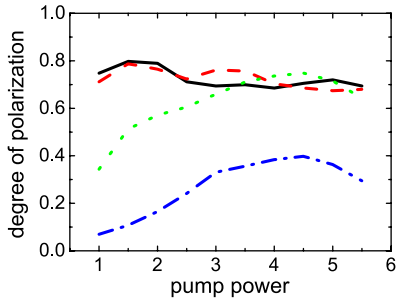

Fig. 6. (Color online) DOP of the output signal beam as function of the pump power for different values of the product $\omega_m T_{NL}$: 0.0002 (black solid curve), 0.02 (red dashed curve), 0.2 (green dotted curve), and 1 (blue dashed–dotted curve). The observation time is $T = 250000 T_{NL}$.

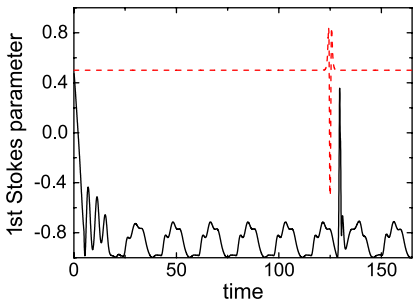

Fig. 7. (Color online) The first Stokes component of the signal beam at the input (red dashed curve) and output (black solid curve) of the medium as a function of time. The polarization burst imposed on the otherwise steady-state input SOP is described by Eqs. (14) and (15). $S_0^- = 3S_0^+$.

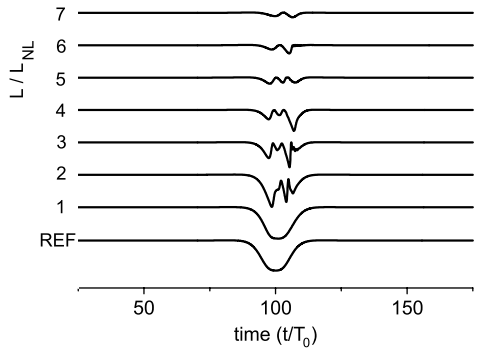

Fig. 8. Illustration of the burst annihilation: the first Stokes component of the signal beam at the output of the medium as the function of time for increasing values of the signal power (from bottom to top). $T_0 = L/v$.

lengths in the total fiber length L). As can be seen, whenever the input signal power is small, the burst propagates through the fiber almost undistorted. However, as the signal power grows larger, the burst is almost entirely annihilated. This compensation is due to shortening of the effective response time T_{NL}, which gradually becomes shorter than the temporal duration of the burst. This plot shows an excellent agreement with the experimental plots presented in Section 4 (see Fig. 12).

4. EXPERIMENTAL RESULTS

In this section, we present an experimental validation of the transient response of the telecom fiber-based NLP that was described in Section 3 by means of numerical simulations. Figure 9 illustrates the experimental setup. The polarization attraction process takes place in a 6.2 km long non-zero dispersion-shifted fiber (NZDSF). Its parameters are: chromatic dispersion $D = -1.5\,\mathrm{ps/nm/km}$ at 1550 nm, Kerr coefficient $1.7\,\mathrm{W^{-1}km^{-1}}$, polarization mode dispersion (PMD) $0.05\,\mathrm{ps/km^{1/2}}$. At both ends of the fiber, circulators ensure injection and rejection of the signal (pump). The 0.7 W signal (1.1 W counterpropagating pump) wave consists of a polarized incoherent wave with spectral linewidth of 100 GHz and a central wavelength of 1544 nm (1548 nm). Note that the spectral linewidth of the signal and pump waves is large enough to avoid any Brillouin backscattering effect within the optical fiber. While the pump wave has a fixed arbitrary SOP, a polarization scrambler is inserted to introduce random polarization fluctuations or polarization events in the input signal wave. Finally, the signal is amplified by means of an erbium-doped fiber amplifier (EDFA) before injection into the optical fiber. At the fiber output, the signal SOP is analyzed in terms of its Stokes vector, which is plotted on the Poincaré sphere by means of a polarization analyzer. In order to monitor the polarization fluctuations of the signal wave in the time domain, a polarizer is inserted at port 3 of the circulator before detection by a standard oscilloscope.

Figure 10 illustrates the polarization attraction efficiency in Approach S. At the input of the fiber, the SOP of the signal randomly fluctuates on a millisecond scale by means of the polarization scrambler. That is to say, we inject a set of $N = 128$ beams fully polarized but all with a random SOP. Consequently, on the Poincaré sphere, all the points are uniformly distributed on the entire sphere [Fig. 10(a)]. To the opposite, whenever the counterpropagating pump wave is injected [Fig. 10(b)], we observe an efficient polarization attraction process that is characterized by a small area of output polarization fluctuations, indicating that the SOP of the output signal is efficiently stabilized. The signal DOP is thus increased by the NLP from 0.15 in Fig. 10(a) to 0.99 in Fig. 10(b).

A. Polarized Signal Beam

As predicted in Section 3, temporal oscillations or even chaos can be observed during the attraction process in a telecom-fiber-based NLP. Indeed, even if the input signal has a constant SOP and a DOP near unity, closed trajectories can be monitored onto the Poincaré sphere at the output of the NLP, which leads to a slight decrease of the DOP. An example of this phenomenon is presented in Fig. 11. A 700 mW CW input signal, which is fully polarized (DOP = 1, i.e., no input time fluctuations) is injected into the fiber. As can be seen on the Poincaré sphere [Fig. 11(a)] as well as on the Stokes parameters [dashed lines in Fig. 11(c)], the input signal SOP is stationary in time. Quite to the opposite, whenever the 1.1 W counterpropagating pump wave is injected into the fiber, a circularlike trajectory can be observed on the signal SOP at the NLP output [Fig. 11(b)]. This corresponds to periodic temporal oscillations of the output signal wave Stokes parameters [Fig. 11(c), solid curves). The periodic evolution of S_1^+, S_2^+, and S_3^+ with a temporal period around 180 μs, which

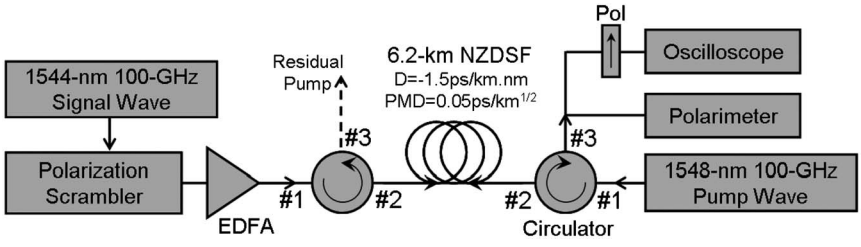

Fig. 9. Experimental setup.

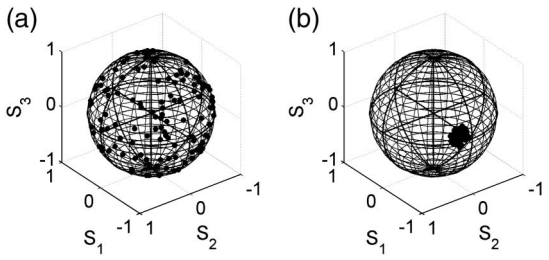

Fig. 10. (a) SOP of the input signal. (b) SOP of the output signal.

corresponds to 60 T_{NL}. We have, therefore, experimentally confirmed the so far unexpected behavior that an NLP can transform a fully polarized wave into a partially polarized beam with periodic polarization oscillations, in good agreement with the theoretical predictions of Subsection 3.A.

B. Burst Annihilation

To experimentally highlight the transient stage of the attraction process, we recorded the evolution of a fast polarization event as a function of signal power, that is to say, as a function of T_{NL}. More precisely, a 30 μs polarization burst was generated on the signal wave by means of the polarization scrambler. The burst was then injected into the fiber along with the counterpropagating pump wave. At the output of the fiber, we finally detected the burst profile in the time domain thanks to a polarizer. The evolution of the burst was then recorded on both axes of the polarizer as a function of signal power for a constant pump power of 1.1 W. The experimental results are illustrated in Fig. 12.

First of all, we may observe a perfect complementarity between the evolution of the burst of both axes, which provide a general overview of the attraction process. At low signal powers (10 mW), the nonlinear length (55 km) is much longer than the fiber length (6 km), so that no attraction process can be developed. As the signal power is increased, the nonlinear length decreases until it reaches the fiber length for signal powers of around 70 mW. At this point, the nonlinear response

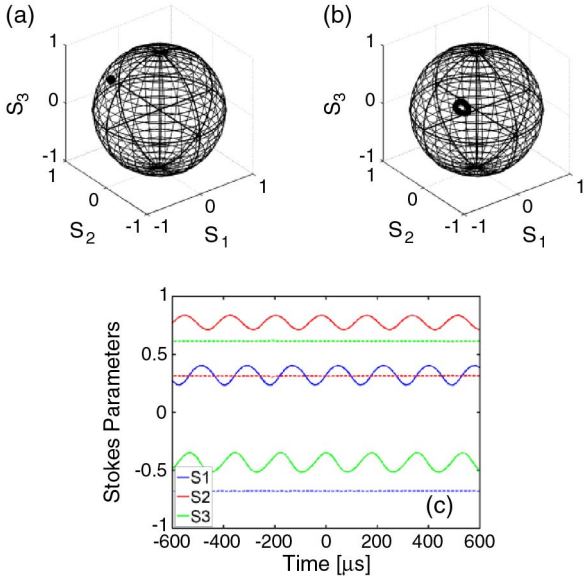

Fig. 11. (Color online) (a) SOP of the input signal. (b) SOP of the output signal. (c) Stokes parameters as a function of time (dashed curve, input; solid curve, output).

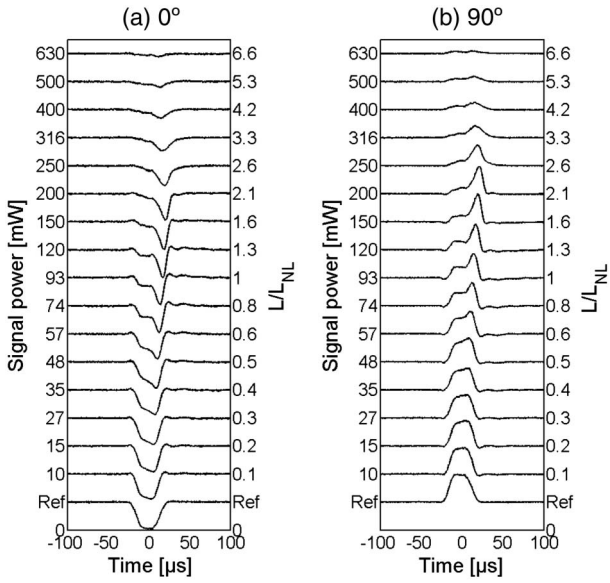

Fig. 12. Evolution of a signal polarization burst as a function of signal average power and detected at the output of the fiber behind a polarizer: along (a) the 0° axis and (b) the orthogonal axis.

time T_{NL} is close to the burst duration and the attraction process begins to develop. A transient regime can then be observed with the formation of a short spike on the falling edge of the burst and even slight oscillations, in good agreement with the theoretical predictions of Fig. 8. As the signal power is further increased, the nonlinear length decreases below 1 km and the polarization attraction process acts in full strength in order to entirely annihilate the polarization burst.

The previous results are confirmed by calculating the ratio of energy on both axes contained in the polarization burst (Fig. 13). Starting with half of the energy on each component, the attraction process leads to the pulling of 95% of the entire burst energy on the 0° axis of the polarizer.

A similar behavior was also experimentally observed whenever the pump (as opposed to the signal) power was increased. Figure 14 presents two examples of compensation of a 30 μs 630 mW polarization burst as a function of pump power. As in Fig. 12, the burst profile was detected at the output of the fiber in the time domain thanks to a polarizer. Once again, a transient regime can be observed with the formation

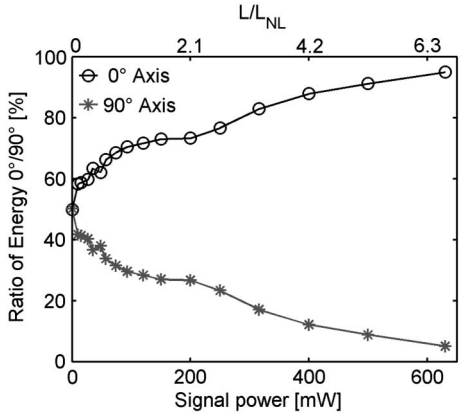

Fig. 13. Ratio of energy on 0°/90° axes contained in the polarization burst.

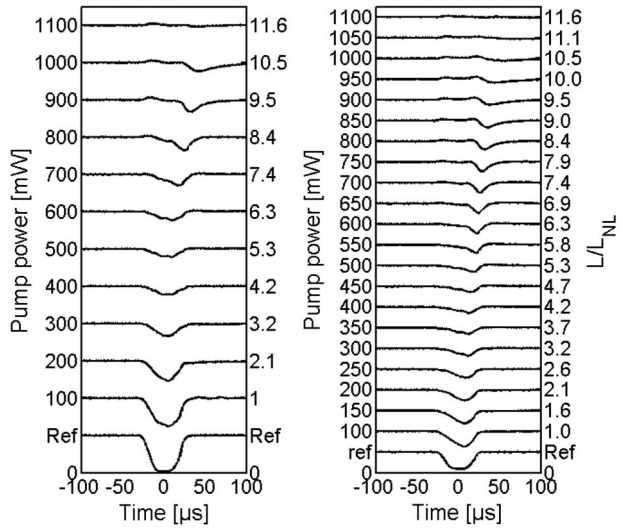

Fig. 14. Two examples of polarization burst evolution as a function of pump power and detected at the output of the fiber behind a polarizer. In contrast to the rest of the paper, here the nonlinear length L_{NL} is defined in terms of the pump power.

of a short spike on the falling edge of the burst. As the pump power increases, around 10 of nonlinear lengths are covered in the fiber, so that the polarization attraction process acts in full strength in order to entirely annihilate the polarization burst.

5. CONCLUSION

In this paper, we studied by both numerical simulations and experiments the transient behavior of telecom fiber-based lossless polarizers. Our main interest is to define the regime for stable long-term behavior of these devices, i.e., when the process of polarization attraction is statistically stationary. In this regime, the statistical characteristics of the polarizer (mean SOP and DOP) do not depend on time and, therefore, represent its universal characteristics. For the polarizer to be in a stationary regime, it is sufficient that the observation time is much longer than the average time that characterizes the time scale of fluctuations of the input signal SOP: $\omega_m T \gg 1$.

We found that the most important time scale to characterize an NLP is its response time T_{NL}. The polarizer exhibits the best performance when fed by signal beams whose input SOP varies in time slowly with respect to its response time. On the other hand, its performance degrades when the rate of fluctuations of the input SOP approaches the characteristic response time T_{NL}. For even faster fluctuation rates, the polarizer is no longer able to perform its function.

For signal power around 1 W and typical for telecom fibers nonlinear coefficients $\gamma \sim 1\,(\mathrm{W}\cdot\mathrm{km})^{-1}$, the nonlinear length $L_{NL} \sim 1$ km and the corresponding response time $T_{NL} \sim 3\,\mu$s. For a nonlinear photonic crystal fiber with $\gamma = 0.1\,(\mathrm{W}\cdot m)^{-1}$, as used in [14], the response time can be reduced to 30 ns. For tellurite photonic crystal fiber with $\gamma = 5.7\,(\mathrm{W}\cdot\mathrm{m})^{-1}$, as used in [15], the response time drops below 1 ns. Overall, higher nonlinear coefficients and correspondingly shorter fibers, like those proposed in [11], are more favorable in applications where the SOP of the signal beam varies faster than $3\,\mu$s.

APPENDIX A: CALCULATION OF THE STATISTICS OF THE STOKES VECTORS IN APPROACH S

As explained in the body of the text, for calculating the response of the NLP in Approach S, we used $N = 110$ or 420 signal beams with different SOPs uniformly distributed over the Poincaré sphere. Then we computed the polarization evolution along the fiber for each of these N realizations, where a pump beam with constant SOP was launched from the opposite end of the fiber. For each realization, we measured $S_1^+(L)$, $S_2^+(L)$, and $S_3^+(L)$. At the end of the simulations, we calculated the mean values:

$$\langle S_i^+(L)\rangle = \frac{1}{N}\sum_{j=1}^{N}[S_i^+(L)]_j, \tag{A1}$$

where $i = 1, 2, 3$. In this form, these averages do not define the mean direction of the Stokes vector on the Poincaré sphere, simply because the sum of squares of these means does not yield the square of the power, $(S_0^+)^2$. The length of the vector satisfies the inequality $\sqrt{\langle S_1^+(L)\rangle + \langle S_2^+(L)\rangle + \langle S_3^+(L)\rangle} \le S_0^+$, and can even be zero for unpolarized light.

However, the information that is contained in the three means is sufficient to restore the direction of the Stokes vector and, moreover, to quantify the degree of polarization of the outcoming signal light. The two angles θ_0 and ϕ_0 (also called circular means) that determine the direction of the Stokes vector on the Poincaré sphere are defined as

$$\theta_0 = \arccos\left(\frac{\langle S_3\rangle}{\sqrt{\langle S_1^+\rangle^2 + \langle S_2^+\rangle^2 + \langle S_3^+\rangle^2}}\right), \tag{A2}$$

$$\phi_0 = a\tan 2(\langle S_2^+\rangle, \langle S_1^+\rangle). \tag{A3}$$

Here,

$$a\tan 2(x,y) = \begin{cases} \arctan(y/x) & x > 0 \\ \pi + \arctan(y/x) & y \ge 0, x < 0 \\ -\pi + \arctan(y/x) & y < 0, x < 0 \\ \pi/2 & y > 0, x = 0 \\ \pi/2 & y < 0, x = 0 \\ \text{undefined} & y = 0, x = 0 \end{cases}. \tag{A4}$$

Finally, the Cartesian coordinates of the Stokes vector are restored as

$$\bar{S}_1 = S_0^+ \sin\theta_0 \cos\phi_0, \tag{A5}$$

$$\bar{S}_2 = S_0^+ \sin\theta_0 \sin\phi_0, \tag{A6}$$

$$\bar{S}_3 = S_0^+ \cos\theta_0. \tag{A7}$$

These values characterize the SOP, while values displayed in Fig. 4 are simple ensemble averages given by the formulas in Eq. (A1).

The DOP is defined as

$$D_S = \sqrt{\langle S_1^+ \rangle^2 + \langle S_2^+ \rangle^2 + \langle S_3^+ \rangle^2}/S_0^+. \quad \text{(A8)}$$

This is the DOP that is used in Approach S, and for this reason supplied with index S. Its values are displayed in Fig. 4.

ACKNOWLEDGMENTS

This work was carried out in the framework of the Research Project of National Interest (PRIN 2008) entitled "Nonlinear cross-polarization interactions in photonic devices and systems," sponsored by Ministero dell'Istruzione, dell'Università e della Ricerca (MIUR).

REFERENCES

1. J. E. Heebner, R. S. Bennink, R. W. Boyd, and R. A. Fisher, "Conversion of unpolarized light to polarized light with greater than 50 efficiency by photorefractive two-beam coupling," Opt. Lett. **25**, 257–259 (2000).
2. J. Fatome, S. Pitois, P. Morin, and G. Millot, "Observation of light-by-light polarization control and stabilization in optical fibre for telecommunication applications," Opt. Express **18**, 15311–15317 (2010).
3. V. V. Kozlov, J. Nuño, and S. Wabnitz, "Theory of lossless polarization attraction in telecommunication fibers," J. Opt. Soc. Am. B **28**, 100–108 (2011).
4. A. Picozzi, "Spontaneous polarization induced by natural thermalization of incoherent light," Opt. Express **16**, 17171–17185 (2008).
5. S. Pitois, G. Millot, and S. Wabnitz, "Nonlinear polarization dynamics of counterpropagating waves in an isotropic optical fiber: theory and experiments," J. Opt. Soc. Am. B **18**, 432–443 (2001).
6. S. Pitois, J. Fatome, and G. Millot, "Polarization attraction using counter-propagating waves in optical fiber at telecommunication wavelengths," Opt. Express **16**, 6646–6651 (2008).
7. S. Pitois, A. Picozzi, G. Millot, H. R. Jauslin, and M. Haelterman, "Polarization and modal attractors in conservative counterpropagating four-wave interaction," Europhys. Lett. **70**, 88–94 (2005).
8. D. Sugny, A. Picozzi, S. Lagrange, and H. R. Jauslin, "Role of singular tori in the dynamics of spatiotemporal nonlinear wave systems," Phys. Rev. Lett. **103**, 034102 (2009).
9. E. Assémat, S. Lagrange, A. Picozzi, H. R. Jauslin, and D. Sugny, "Complete nonlinear polarization control in an optical fiber system," Opt. Lett. **35**, 2025 (2010).
10. S. Lagrange, D. Sugny, A. Picozzi, and H. R. Jauslin, "Singular tori as attractors of four-wave-interaction systems," Phys. Rev. E **81**, 016202 (2010).
11. V. V. Kozlov and S. Wabnitz, "Theoretical study of polarization attraction in high birefringence and spun fibers," Opt. Lett. **35**, 3949–3951 (2010).
12. C. M. de Sterke, K. R. Jackson, and B. D. Robert, "Nonlinear coupled-mode equations on a finite interval: a numerical procedure," J. Opt. Soc. Am. B **8**, 403–412 (1991).
13. B. Daino and S. Wabnitz, "Polarization domains and instabilities in nonlinear optical fibers," Phys. Lett. A **182**, 289–293 (1993).
14. A. A. Amorim, M. V. Tognetti, P. Oliveira, J. L. Silva, L. M. Bernardo, F. X. Kärtner, and H. M. Crespo, "Sub-two-cycle pulses by soliton self-compression in highly nonlinear photonic crystal fibers," Opt. Lett. **34**, 3851–3853 (2009).
15. M. Liao, C. Chaudhari, G. I. Qin X. Yan, T. Suzuki, and Y. Ohishi, "Tellurite microstructure fibers with small hexagonal core for supercontinuum generation," Opt. Express **17**, 12174–12182 (2009).